Available online at www.sciencedirect.com
ScienceDirect
Ceramics International 38 (2012) 301–310
CERAMICS INTERNATIONAL
www.elsevier.com/locate/ceramint

# Effects of the starting materials and mechanochemical activation on the properties of solid-state reacted $Li_4Ti_5O_{12}$ for lithium ion batteries

Chang-Hoon Hong [a], Alfian Noviyanto [a], Ji Heon Ryu [b], Jaemyung Kim [c], Dang-Hyok Yoon [a,*]

[a] School of Materials Science and Engineering, Yeungnam University, Gyeongsan 712-749, Republic of Korea
[b] Graduate School of Knowledge-Based Technology & Energy, Korea Polytechnic University, Siheung 429-793, Republic of Korea
[c] Energy Development Team, Corporate R&D Center, Samsung SDI, Yongin 446-577, Republic of Korea

Received 13 April 2011; received in revised form 30 June 2011; accepted 5 July 2011
Available online 18th July 2011

**Abstract**

$Li_4Ti_5O_{12}$ was synthesized by a solid-state reaction between $Li_2CO_3$ and $TiO_2$ for applications in lithium ion batteries. The effects of the $TiO_2$ phase and mechanochemical activation on the $Li_4Ti_5O_{12}$ particles as well as the corresponding electrochemical properties were investigated. Rutile $TiO_2$ was more desirable in acquiring high purity $Li_4Ti_5O_{12}$ than anatase due to the anatase to rutile phase transformation, which was found to be more rigid in the solid-state reaction than the intact rutile phase. Mechanochemical activation of the starting materials was effective in decreasing the reaction temperature and particle size as well as increasing the $Li_4Ti_5O_{12}$ content. The specific capacity depended significantly on the $Li_4Ti_5O_{12}$ content, whereas the rate capability improved with decreasing particle size due to the enhanced contact area and reduced diffusion path. Overall, a 200 nm-sized $Li_4Ti_5O_{12}$ powder with a specific capacity of 165 mAh/g could be synthesized by optimizing the milling method and starting materials.


*Keywords:* E. Batteries; Solid-state reaction; Mechanochemical activation; $Li_4Ti_5O_{12}$; Electrochemical properties

## 1. Introduction

$Li_4Ti_5O_{12}$ is a promising anode material for high power Li-ion batteries owing to its good cycle performance and little structural change during the $Li^+$ intercalation and de-intercalation process with a theoretical capacity of 175 mAh/g [1–5]. Since it shows a flat Li insertion potential of 1.55 V versus Li/$Li^+$, which is higher than the reduction potentials of common electrolyte solvents, it does not form a solid electrolyte interface during operation [2,6]. These properties can be a great merit for electric and/or hybrid vehicle applications of Li-ion batteries, which demand high power operation and long-term stability [7,8].

To produce high rate Li-ion batteries, a very fine active material is more desirable than a coarse one due to its shorter $Li^+$ diffusion path and greater electrode–electrolyte contact area for $Li^+$ intercalation and de-intercalation [9–11]. On the other hand, the properties of the particles depend significantly on the synthetic process and starting materials, which lead to final products with range of sizes and morphologies. Therefore, considerable effort is being made to enhance the electrochemical performance of batteries by optimizing the electrode materials, including the utilization of various synthetic methods, doping and coating with other materials [12–18]. Generally, a spinel-type $Li_4Ti_5O_{12}$ is synthesized by an economic solid-state reaction using $TiO_2$ and $Li_2CO_3$, which generally results in a significant amount of agglomeration and a coarse particle size. This is why wet chemical methods, such as hydrothermal and coprecipitation, have been attempted despite their high cost [19–22].

The synthesis of fine ceramic powders through a solid-state reaction with the aid of an advanced high energy mill was reported recently [23,24]. Compared to a conventional ball mill, the modern high energy mill shows much higher milling efficiency owing to its high speed rotor turning at up to several thousand rotations per minute. Their high energy input along with the use of small grinding media enables the achievement of very small particle sizes in a very short processing time

* Corresponding author. Tel.: +82 538102561; fax: +82 538104628.
*E-mail address:* dhyoon@ynu.ac.kr (D.-H. Yoon).

0272-8842/$36.00 
doi:10.1016/j.ceramint.2011.07.007

[24,25]. The mechanochemical activation by heavy milling is the key process in the solid-state synthesis of nano-sized ceramic powders, for example $BaTiO_3$ [23,24], which alters the physicochemical properties of the starting materials. Finely milled starting materials enhance the solid-state reaction due to their high activity and decrease the reaction temperature and final particle size.

To the best of the authors' knowledge, there are no reports on the effect of mechanochemical activation for the starting materials on the formation of $Li_4Ti_5O_{12}$ powder. With this background, this study compared the effects of milling methods (ball milling and high energy milling) on the properties of $Li_4Ti_5O_{12}$ powder and the corresponding electrochemical properties. In addition, the effects of two different starting $TiO_2$ phases, i.e., anatase- and rutile-phased $TiO_2$, were also examined.

## 2. Experimental procedure

### 2.1. Starting materials

Commercial $Li_2CO_3$ and $TiO_2$ powders were used as Li- and Ti-precursors for $Li_4Ti_5O_{12}$ synthesis, respectively, where two different types of $TiO_2$ powders, i.e., anatase- and rutile-phase, were used to examine the phase effects. Table 1 lists the characteristics of the starting materials, including the manufacturer, mean particle size and purity.

### 2.2. Synthesis of the spinel $Li_4Ti_5O_{12}$

To synthesize 100 g of $Li_4Ti_5O_{12}$ powder, 32.19 g of $Li_2CO_3$ and 86.98 g of $TiO_2$, which correspond to a Li/Ti stoichiometric ratio of 4/5, were mixed with 200 g of de-ionized water after adding 2 wt.% of the ammonium salt of polycarboxylic acid (Cerasperse 5468-CF, San Nopco, Korea) with respect to the ceramic powder, as a dispersant. Formulated mixtures containing 2 different $TiO_2$ powders were exposed to high energy milling (MiniCer, Netzsch, Germany) for 3 h at a rotor speed of 3000 rpm with 0.4 mm $ZrO_2$ beads. The mixtures with the same formulation were also ball-milled for 24 h using 5 mm $ZrO_2$ balls for comparison. The four types of slurries were dried after milling at 100 °C in a rotary evaporator for uniform mixing. The dried powders are named AB, AH, RB and RH depending on the $TiO_2$ type and milling method, where A and R stand for anatase- and rutile-$TiO_2$, and B and H for ball-milled and high energy-milled, respectively. Each dried powder was heat-treated at 700, 800 and 900 °C for 3 h in air at a heating rate of 3 °C/min.

Table 1
Characteristics of the starting materials used in this study.

| Materials | Manufacturer | $D_{50}$ (μm) | Purity | Note |
|---|---|---|---|---|
| $Li_2CO_3$ | New Well, Korea | 3.80 | >99.9 | Broad size distribution |
| $TiO_2$ (anatase) | Hang Zhou Wan Jing, China | 0.08 | >99.0 | Highly agglomerated |
| $TiO_2$ (rutile) | Toho Titanium, Japan | 0.78 | >99.9 | 3.5 wt.% anatase $TiO_2$ contained |

### 2.3. Characterization of the particles

The dispersion stability of the particles associated with wet milling was examined by measuring the zeta potentials of the starting materials using an electroacoustic-type zeta potential analyzer (Zeta Probe, Colloidal Dynamics, USA) with and without a dispersant after adjusting the pH of the slurry using $NH_4OH$ and HCl. The morphologies of the starting materials before and after milling were characterized by scanning electron microscopy (SEM: S-4800, Hitachi using 15 kV and 10 μA with the working distance of 5–8 mm, Hitachi). The thermal decomposition behavior of 4 different combinations were examined by thermogravimetric analysis (TGA: SDT Q600, TA Instruments, USA) in a flowing air atmosphere at temperatures ranging from room temperature to 1000 °C with a heating rate of 5 °C/min. Room temperature XRD (RT-XRD: X'Pert-PRO MPD, Panalytical using Cu $K_\alpha$ line, 40 kV and 30 mA) and Rietveld refinement were performed for quantitative phase verification after heat treatment. In addition, high temperature XRD (HT-XRD: D/MAX-RB, Rigaku using Cu $K_\alpha$ line, 40 kV and 300 mA) was performed for the AH combination to confirm in situ the phases generated during heat treatment. For the measurements, the samples were heat-treated from room temperature to 800 °C in 100 °C steps and held at each measurement temperature for 3 min.

### 2.4. Electrochemical testing

To evaluate the electrochemical properties, an electrode paste composed of 80 wt.% $Li_4Ti_5O_{12}$, 10 wt.% Denka black and 10 wt.% poly(vinylidene fluoride) (PVdF, KF1300) was mixed and dispersed. The paste was then screen-printed on Al foil to form an electrode. The electrode plate was then pressed to enhance the interparticle contact and to ensure a better adhesion to the current collector. Coin-type half-cells (CR2032) were assembled with the composite electrode, Li foil as a counter electrode, and polyethylene film as a separator. The electrolyte used was 1.3 M $LiPF_6$ dissolved in a mixture of ethylene carbonate and ethylmethyl carbonate with a volume ratio of 1/2. The cell assembly was performed in a glove box filled with Ar gas, and the electrode was dried under vacuum at 120 °C to remove the moisture before filling the electrolyte. The galvanostatic charge–discharge measurements were performed in a potential range of 1.0–2.5 V (versus $Li/Li^+$) at different current conditions of 0.1*C* (17.5 mA/g)–4.0*C* (700 mA/g). The cells were charged and discharged for three cycles at each current density at 25 °C.

## 3. Results and discussion

### 3.1. Starting materials and their dispersion stability

Since a solid-state reaction occurs at the contact points of the starting materials, the use of very fine and uniformly dispersed

$Li_2CO_3$ and $TiO_2$ is very important for enhancing the reaction rate and decreasing the processing temperature. According to the SEM images of the starting materials shown in Fig. 1, $Li_2CO_3$ and rutile $TiO_2$ have a relatively large particle size of 3.80 and 0.78 μm, respectively, whereas anatase $TiO_2$ has a very fine primary particle size of approximately 80 nm, even though it exists in a highly agglomerated state. Therefore, efficient milling of the starting materials to obtain fine and highly dispersed particles appears to be necessary.

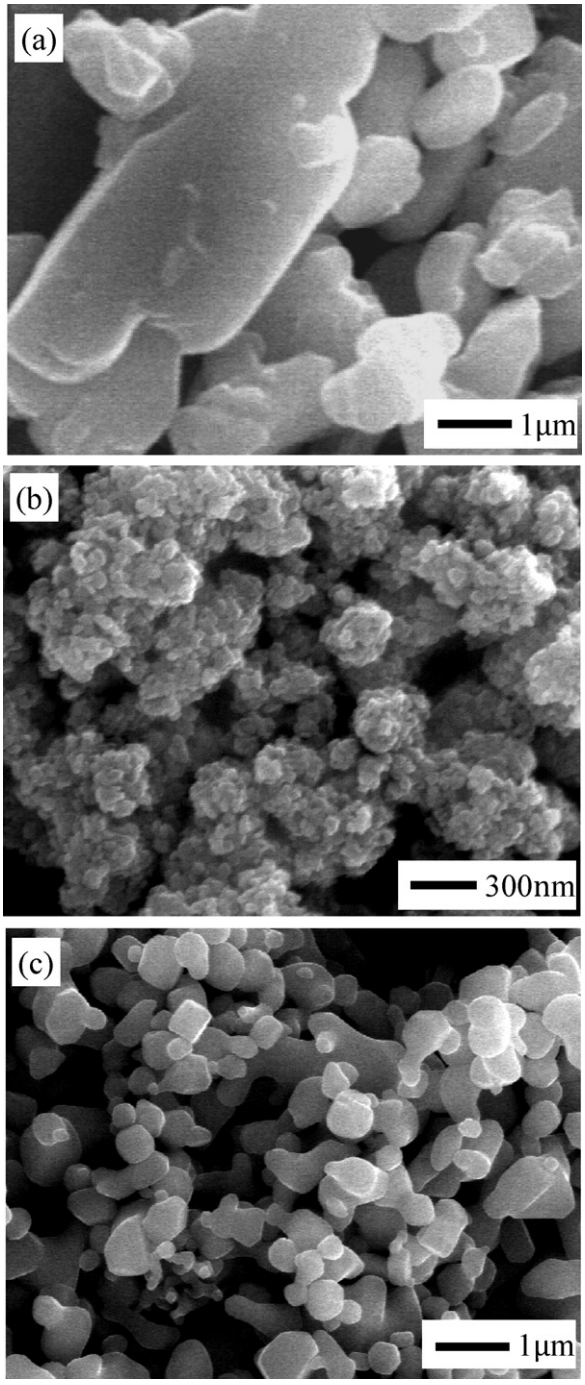


Fig. 1. SEM images of the starting materials: (a) $Li_2CO_3$, (b) anatase $TiO_2$, and (c) rutile $TiO_2$.

Although the agglomerated and coarse particles can be broken down by shear force during wet milling, in the absence of long-term dispersion stability, agglomeration will occur again when the shear is removed. The dispersion stability can be achieved by electrostatic and steric mechanisms, which prevent the particles from approaching each other using electrostatic repulsive force and hindrance by the adsorption of polymeric molecules on the particle surface, respectively. To check the stability, the zeta potentials of the starting materials were measured in water with and without a dispersant as a function of pH (Fig. 2). $Li_2CO_3$ shows a high zeta potential of approximately +100 mV regardless the presence of a dispersant. The pH of the $Li_2CO_3$ slurry remained high despite the addition of HCl because $CO_3^{2-}$ acts as a buffer [26]. The isoelectric points (IEPs) of anatase and rutile $TiO_2$ without a dispersant were pH = 6.0 and 6.1, respectively, whereas those with a dispersant decreased to pH = 3.4 and 2.9 because of the anionic nature of Cerasperse 5468CF. Since the pH of the mixed $Li_2CO_3$ and $TiO_2$ slurries with the dispersant are approximately 9–10 for both $TiO_2$ phases, there is a large difference in zeta potential between $Li_2CO_3$ and $TiO_2$, suggesting an efficient electrostatic repulsion and attraction forces between the same and different types of particles in this pH region, respectively. Moreover, steric repulsion by a polymeric dispersant as well as heterocoagulation [27] between $Li_2CO_3$ and $TiO_2$ by different surface charges are expected.

### 3.2. Effects of milling on solid-state reaction

Fig. 3 shows SEM images of the starting materials after 2 types of milling for different combinations. The AB combination still showed coarse $Li_2CO_3$ particles with agglomerated anatase-phased $TiO_2$ after 24 h of ball milling, whereas AH showed finely milled and uniform particles after 3 h of high energy milling. A similar trend was observed with RB and RH, even though the overall particle sizes were coarser than AB and AH due to the initial large particle size of rutile $TiO_2$. This

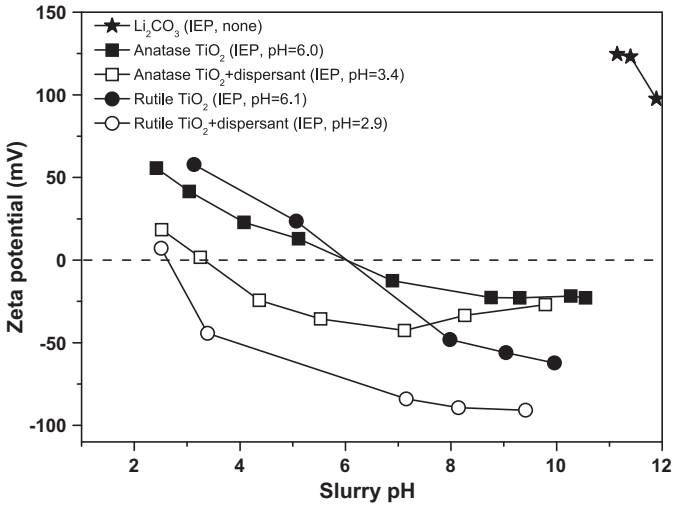


Fig. 2. Zeta potential behavior of the starting materials as a function of the slurry pH.

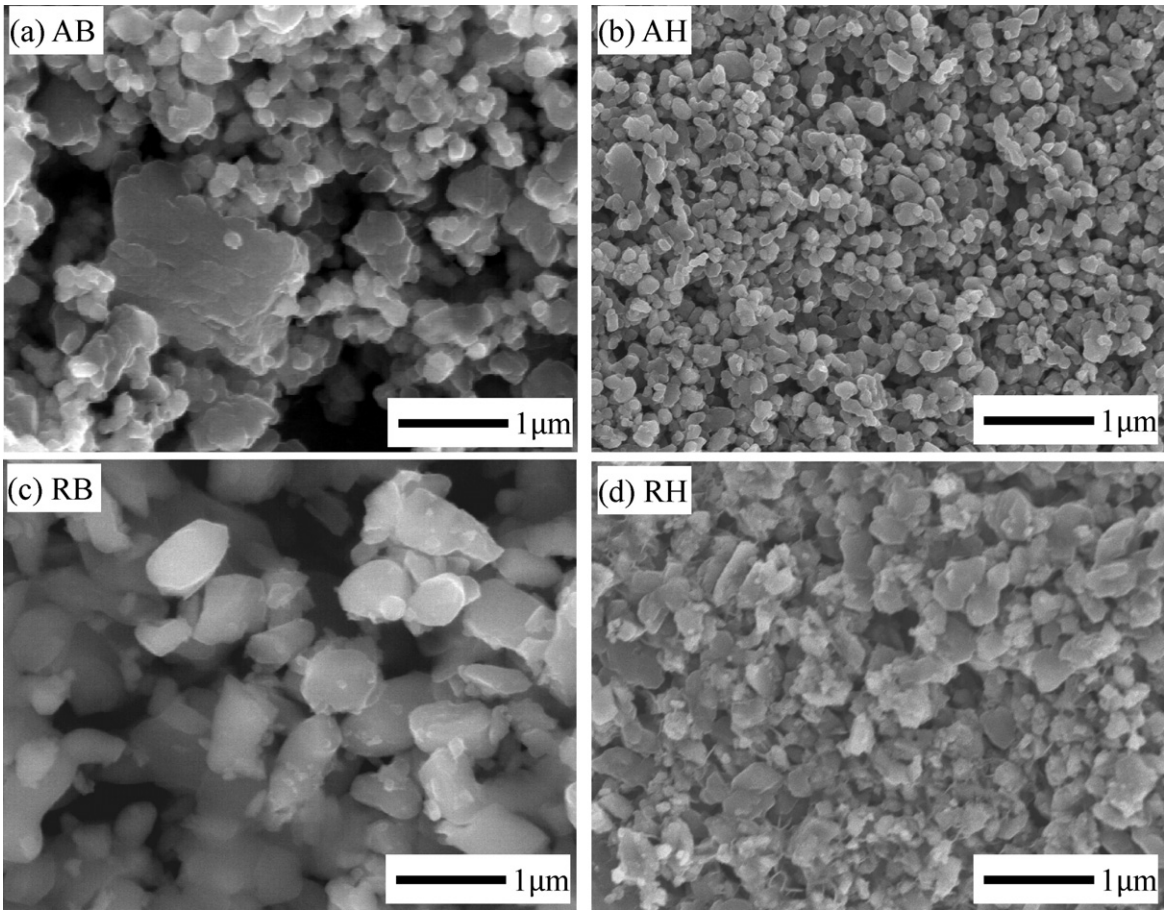


Fig. 3. SEM images of the starting materials after two types of milling (A: anatase $TiO_2$ + $Li_2CO_3$, R: rutile $TiO_2$ + $Li_2CO_3$, B: 24 h of ball milling, H: 3 h of high energy milling).

efficient milling for the starting materials using a high energy mill is expected to decrease the reaction temperature further due to homogeneous mixing and mechanochemical activation.

Fig. 4 shows the TGA results at a heating rate of 5 °C/min in air for 4 different combinations, showing drastic weight loss between 300 and 700 °C. AB, AH and RH show similar weight loss behavior with a total loss of >18.4%, while RB shows 16.7% loss at temperatures 100–200 °C higher than the other samples. This difference in temperature for weight loss can be explained by the effects of the different $TiO_2$ phase and milling method. Regarding the effect of $TiO_2$ phase, anatase with a lower theoretical density (3.90 g/cm$^3$) and finer particle size can have higher activity for a solid-state reaction owing to its looser structure and shorter diffusion path than rutile with a higher density (4.23 g/cm$^3$) and coarser particle size. A comparison of the RB and RH combination showed that mechanochemical activation by high energy milling also decreases the reaction temperature. On the other hand, the effect of mechanochemical activation for fine anatase $TiO_2$ on the temperature decrease was smaller than that for rutile, which can be explained by the high initial activity of fine anatase $TiO_2$ before milling. The solid-state reaction between $Li_2CO_3$ and $TiO_2$ is explained by Eq. (1):

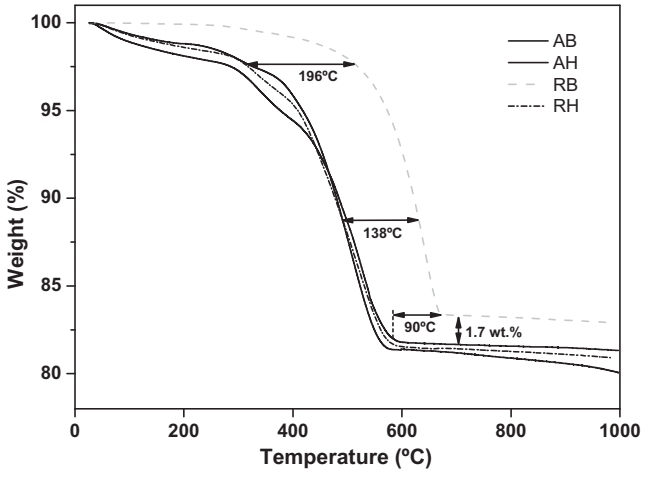


Fig. 4. TGA results for the 4 different combinations, showing the effect of mechanochemical activation by high energy milling for the rutile-phase $TiO_2$ and $Li_2CO_3$ combination.

$$2Li_2CO_3 + 5TiO_2 \rightarrow Li_4Ti_5O_{12} + 2CO_2 \quad (1)$$

where 16.1% of the weight loss is expected due to $CO_2$ evolution. RB shows similar weight loss of 16.7%, whereas the others show >18.0% because of the larger amount of adsorbed water on the fine particles.

### 3.3. XRD results and the phase transformation of $TiO_2$

Fig. 5 shows XRD patterns of 4 different samples heat-treated at (a) 700 °C and (b) 800 °C for 3 h in air. Although most reports used heat treatment at ≥800 °C for ≥12 h for $Li_4Ti_5O_{12}$ formation [3–6,13–18,28,29], the samples were kept at the target temperature for only 3 h to examine the effects of mechanochemical activation and starting materials. According to Fig. 5(a), the high energy-milled powder showed clearer $Li_4Ti_5O_{12}$ peaks than the ball-milled samples. On the other hand, virtually no XRD peaks for $Li_4Ti_5O_{12}$ were found for the samples prepared with rutile $TiO_2$, regardless of the types of milling, whereas the peaks for the intermediate $Li_2TiO_3$ compound were found. Moreover, AH prepared with anatase $TiO_2$ contained rutile-phase $TiO_2$, which was not observed with AB at 700 °C, indicating an anatase- to rutile $TiO_2$ phase transformation in the AH sample. The effectiveness of high energy milling on solid-state reaction of $Li_4Ti_5O_{12}$ can still be found at 800 °C from the relatively higher $Li_4Ti_5O_{12}$ peak heights, i.e., higher crystallinity, of the high energy-milled samples than those ball-milled, as shown in Fig. 5(b). The peaks for transformed rutile $TiO_2$ were observed in both AB and AH at 27.5° 2$\theta$. The lower temperature for the anatase- to rutile $TiO_2$ transformation in the AH sample than the AB sample was

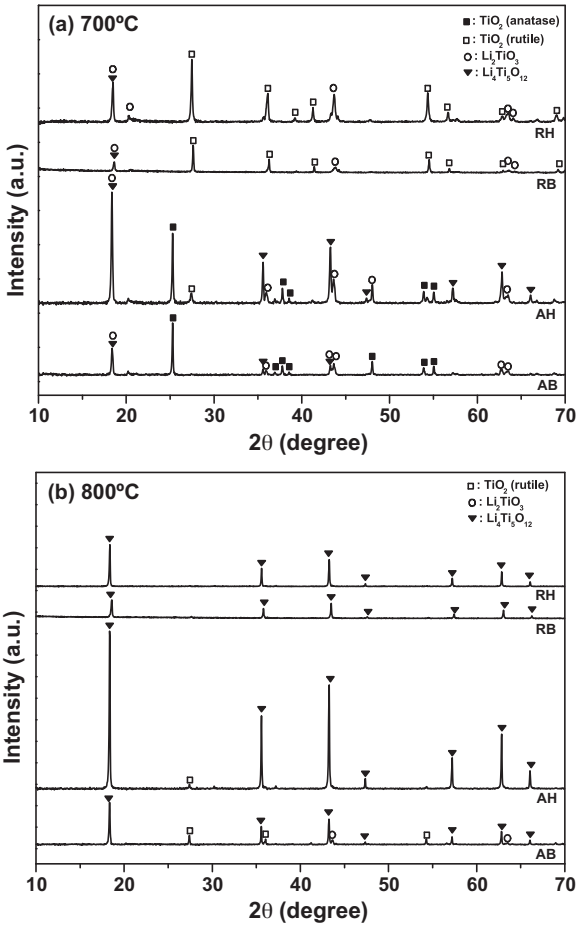


Fig. 5. XRD patterns of the samples after heat treatment at (a) 700 and (c) 800 °C using 4 different powder samples.

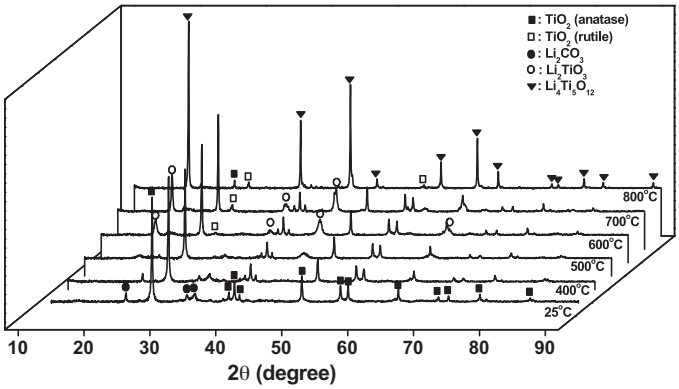


Fig. 6. HT-XRD patterns of the AH combination.

attributed to the effect of mechanochemical activation. Although $Li_4Ti_5O_{12}$ peaks are only were found when anatase $TiO_2$ was used because of the phase transformation. In addition, the peaks for $Li_2TiO_3$ were also observed in the AB sample due to the poor activity of the starting materials after heat treatment at 800 °C. Although the XRD patterns are not shown, the rutile $TiO_2$ that formed from anatase still remained after heat treatment at 900 °C. The rutile $TiO_2$ transformed from anatase appears to be more rigid than the intact rutile $TiO_2$, which hinders the formation of $Li_4Ti_5O_{12}$ even at 900 °C.

HT-XRD was performed from room temperature to 800 °C in 100 °C steps for AH combination to observe this anatase- to rutile $TiO_2$ transformation in situ, as shown in Fig. 6. The starting materials were maintained up to 500 °C, whereas an intermediate phase of $Li_2TiO_3$ and the onset of rutile $TiO_2$ at 27.5° 2$\theta$ was observed at 600 °C. This transformed rutile $TiO_2$ remained at 800 °C, even though $Li_2TiO_3$ had already transformed to $Li_4Ti_5O_{12}$ at this temperature.

The typical reported temperature for the anatase- to rutile $TiO_2$ transformation is higher than 700 °C [30–33]. Therefore, a supplementary test between pure anatase $TiO_2$ and the AH combination was performed to confirm the phase transformation. According to the XRD patterns in Fig. 7(a), the anatase- to rutile $TiO_2$ phase transformation begins from 900 °C, and rutile $TiO_2$ becomes a major phase at 1000 °C. On the other hand, this transformation temperature decreases to 600 °C when anatase $TiO_2$ is mixed with $Li_2CO_3$, as shown in Fig. 7(b). This decrease in $TiO_2$ transformation temperature can be explained by the catalytic effect of $Li_2CO_3$ and the mechanochemical activation by high energy milling.

### 3.4. $Li_4Ti_5O_{12}$ properties and the results of Rietveld simulation

Fig. 8 shows SEM images of the $Li_4Ti_5O_{12}$ powders synthesized at 800 and 900 °C for 4 different combinations. The mean particle size of the AB, AH, RB and RH samples at 800 °C were 271, 204, 349 and 276 nm, respectively. The particle size of $Li_4Ti_5O_{12}$ prepared with anatase $TiO_2$ and high energy milling was smaller than that prepared with rutile one and ball milling. Although the overall particle size increased, the same trend was observed for the samples heat-treated at

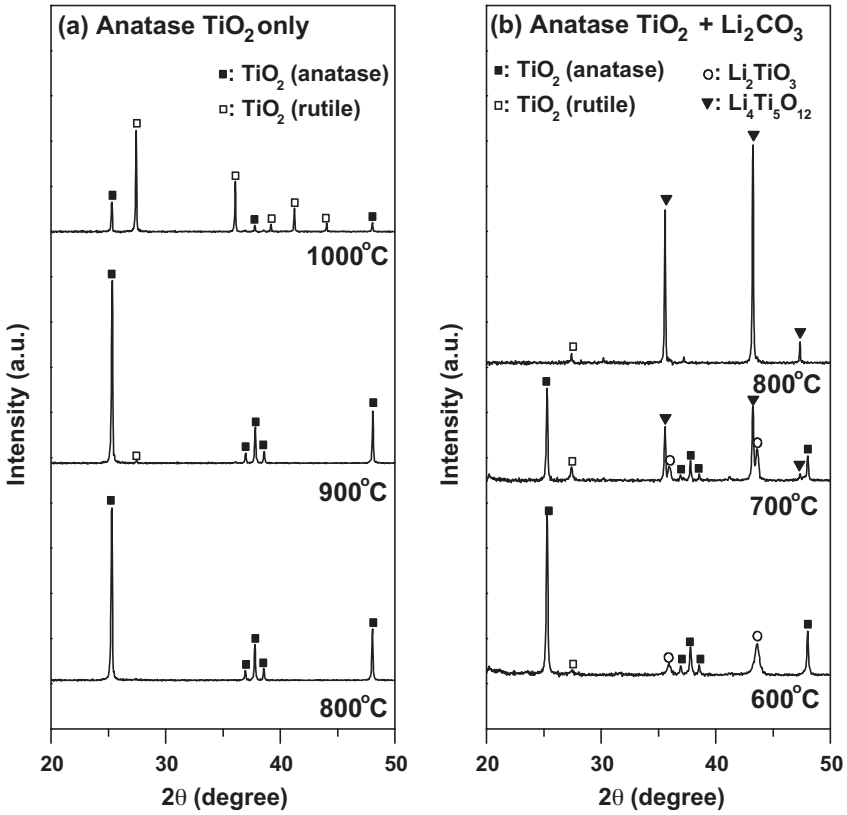


Fig. 7. XRD patterns showing the anatase- to rutile-$TiO_2$ transition temperature at different conditions.

900 °C. In addition, more polygonal shaped particles with ledges, indicating higher crystallinity, were observed in the samples prepared by high energy milling than those by ball milling. From these observations, it can be concluded that fine starting materials are favorable for acquiring fine $Li_4Ti_5O_{12}$ particles with high crystallinity, which can be achieved by the mechanochemical activation of $TiO_2$ and $Li_2CO_3$.

Table 2 summarizes the phase content calculated by a Rietveld simulation for 4 different combinations after heat treatment at 700, 800 and 900 °C. Although the characteristic XRD peaks for rutile $TiO_2$ cannot be observed for the RH and RB samples after the 800 °C treatment, as shown in Fig. 5(b), the simulation revealed the existence of a small amount of this phase. According to this table, a larger amount of $Li_4Ti_5O_{12}$ was found for the samples prepared with anatase $TiO_2$ and high energy milling than those prepared with rutile and ball milling at the initial $Li_4Ti_5O_{12}$ formation temperature of 700 °C. This was attributed to the loose anatase $TiO_2$ structure and high activity of the starting materials as a result of mechanochemical activation. However, after 800 and 900 °C treatments, the content of $Li_4Ti_5O_{12}$ in the samples prepared with rutile-phased $TiO_2$ was higher than those prepared with anatase, which is the opposite trend from that observed at 700 °C. On the other hand, the effect of high energy milling was maintained over the entire temperature ranges. This appears to be the result of the anatase to rutile phase transformation, where the transformed rutile phase is more rigid than the intact rutile $TiO_2$, which hinders the formation of $Li_4Ti_5O_{12}$, as indicated by the XRD patterns in Fig. 5.

### 3.5. Electrochemical properties

Fig. 9(a) and (b) shows the charge/discharge profiles in the third cycle at 0.1*C* for $Li_4Ti_5O_{12}$ electrodes prepared with anatase- and rutile $TiO_2$, respectively. According to Fig. 9(a), the discharge capacity of $Li_4Ti_5O_{12}$ electrodes prepared with anatase $TiO_2$ depends significantly on the milling method and heat treatment temperature. For example, the specific capacity of the AB sample after the 800 °C treatment was 102.4 mAh/g, whereas the AH sample shows the highest value of 165.3 mAh/g after treatment at the same temperature. The capacity of the 900 °C treated samples was higher the AB sample, but slightly lower for the AH sample compared to that of the 800 °C treated samples. On the other hand, the samples prepared with rutile $TiO_2$ showed a high specific capacity of 160.6–165.1 mAh/g regardless of the temperature and milling method, as shown in Fig. 9(b). When the results shown in Fig. 9 were compared with the phase contents in Table 2, a strong correlation was found between the specific capacity and $Li_4Ti_5O_{12}$ content. Since $Li_4Ti_5O_{12}$ is the main phase that can participate in charge storage among the many phases shown in Table 2, higher $Li_4Ti_5O_{12}$ content of the final product is desirable for increasing the specific capacity.

Fig. 10 shows the rate performance of a half-cell with $Li_4Ti_5O_{12}$ electrodes at different *C*-rates. The *C*-rates were varied in the order of 0.1–0.2–0.5–1.0–2.0–4.0–0.1*C* with 3 cycles at each rate and a rest time of 10 min after each measurement. Although all samples showed good cyclability at each *C*-rate along with the complete capacity recovery to the

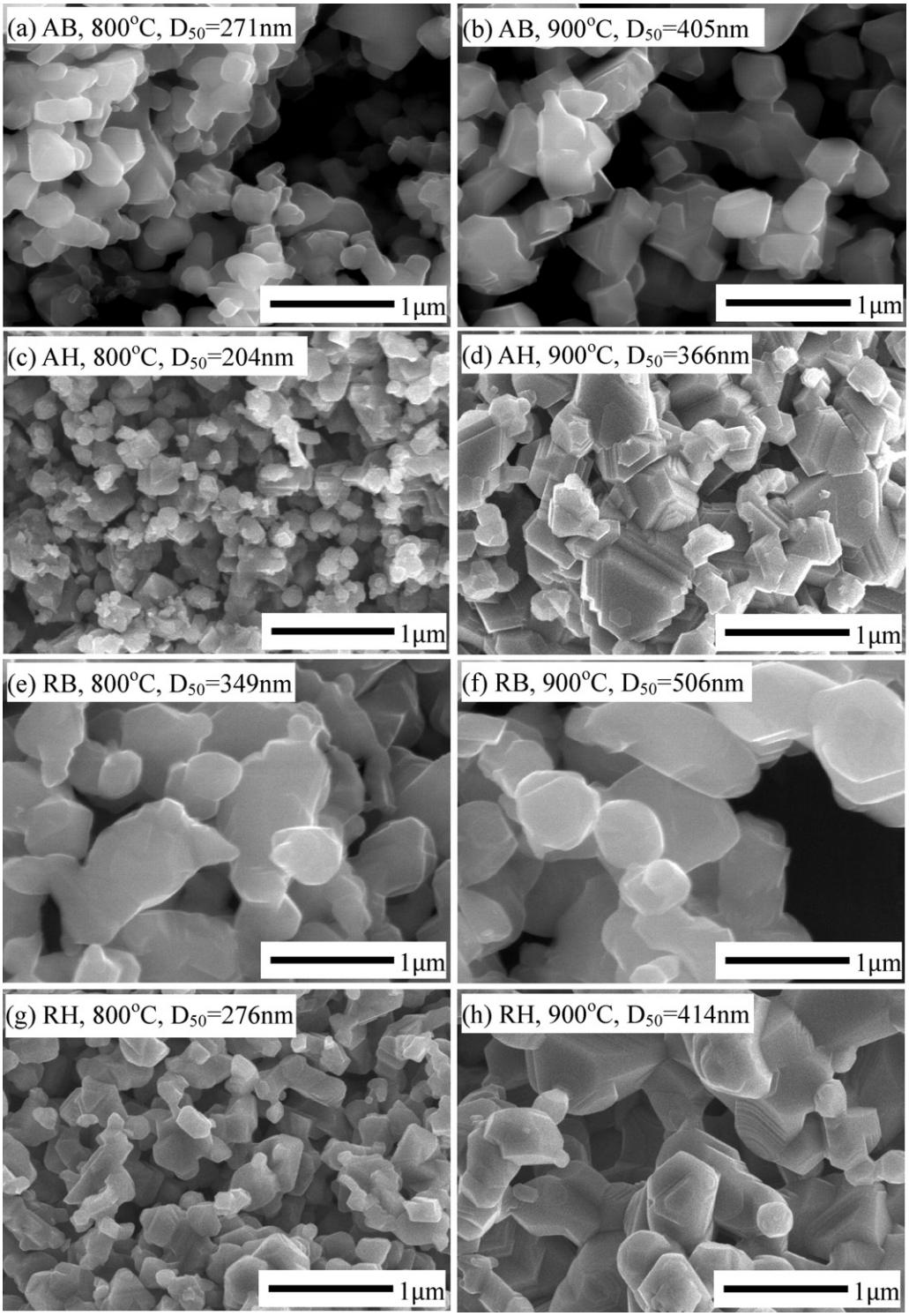


Fig. 8. SEM images of $Li_4Ti_5O_{12}$ particles after heat treatment at 800 and 900 °C for the different combinations.

initial value at the final 0.1*C*, the rate capability depends on the type of samples. The rate capability of the electrodes prepared with $Li_4Ti_5O_{12}$ heat-treated at 800 °C appears to be better than those treated at 900 °C, regardless the types of starting materials and milling methods, as shown in Fig. 11. The RH sample after heat treatment at 800 °C showed the best rate capability at 4*C*, according to Fig. 11. Although the AB sample treated at 800 °C showed the second highest rate capability, it showed the lowest specific capacity of 102.4 mAh/g, as shown in Fig. 9. Therefore, no correlation between the specific capacity and rate capability is expected. A small $Li_4Ti_5O_{12}$ particle size appears to be the main factor for achieving a high rate capability by promoting the $Li^+$ intercalation and de-intercalation process through the short diffusion path and enhanced contact area between $Li_4Ti_5O_{12}$ and the electrolyte.

Table 2
Phase content based on a Rietveld simulation as a function of the temperature for different starting materials and milling methods. The abbreviation for each sample is shown in parenthesis.

| Starting materials | Milling method | Phase | Contents (wt.%) | | |
|---|---|---|---|---|---|
| | | | 700 °C | 800 °C | 900 °C |
| $Li_2CO_3$ + anatase $TiO_2$ | Ball milling (AB) | Rutile $TiO_2$ | – | 17.1 | 7.6 |
| | | Anatase $TiO_2$ | 44.5 | – | – |
| | | $Li_2TiO_3$ | 31.2 | 1.6 | 0.8 |
| | | $Li_4Ti_5O_{12}$ | 24.4 | 81.3 | 91.7 |
| | High energy milling (AH) | Rutile $TiO_2$ | 6.2 | 3.1 | 1.8 |
| | | Anatase $TiO_2$ | 23.4 | – | – |
| | | $Li_2TiO_3$ | 16.7 | 0.4 | – |
| | | $Li_4Ti_5O_{12}$ | 53.8 | 96.5 | 98.2 |
| $Li_2CO_3$ + rutile $TiO_2$ | Ball milling (RB) | Rutile $TiO_2$ | 58.3 | 2.6 | 0.8 |
| | | Anatase $TiO_2$ | – | – | – |
| | | $Li_2TiO_3$ | 41.7 | 0.3 | – |
| | | $Li_4Ti_5O_{12}$ | – | 97.1 | 99.2 |
| | High energy milling (RH) | Rutile $TiO_2$ | 52.5 | 1.2 | – |
| | | Anatase $TiO_2$ | – | 0.3 | – |
| | | $Li_2TiO_3$ | 34.7 | – | – |
| | | $Li_4Ti_5O_{12}$ | 12.8 | 98.5 | 100 |

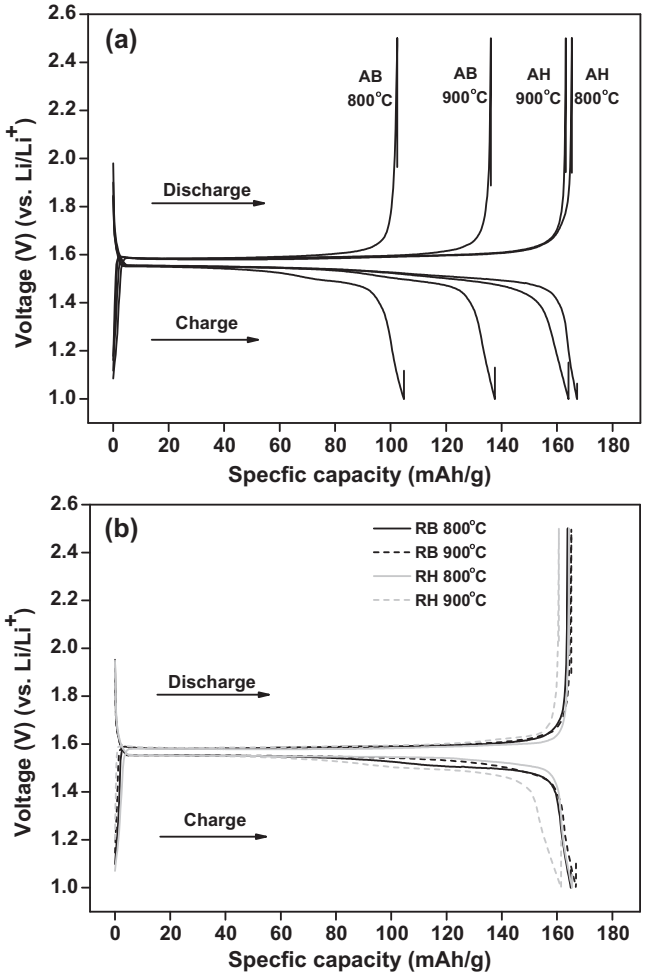


Fig. 9. Voltage profiles for charge and discharge of the $Li_4Ti_5O_{12}$ electrodes at the third cycle with a charging/discharging rate of 0.1*C*.

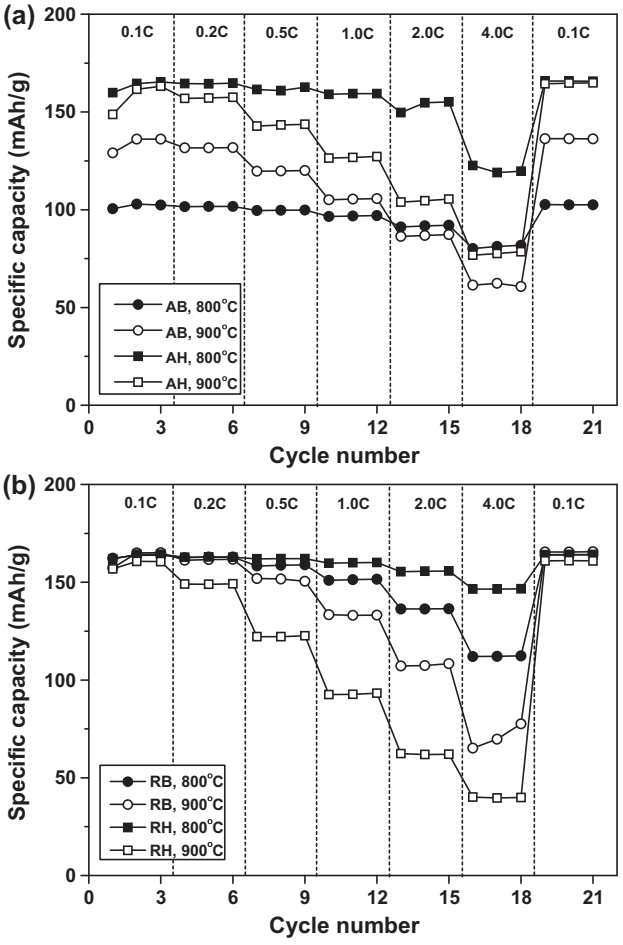


Fig. 10. Rate capabilities of the $Li_4Ti_5O_{12}$ electrodes prepared using different starting materials and milling methods at different charge–discharge rates.

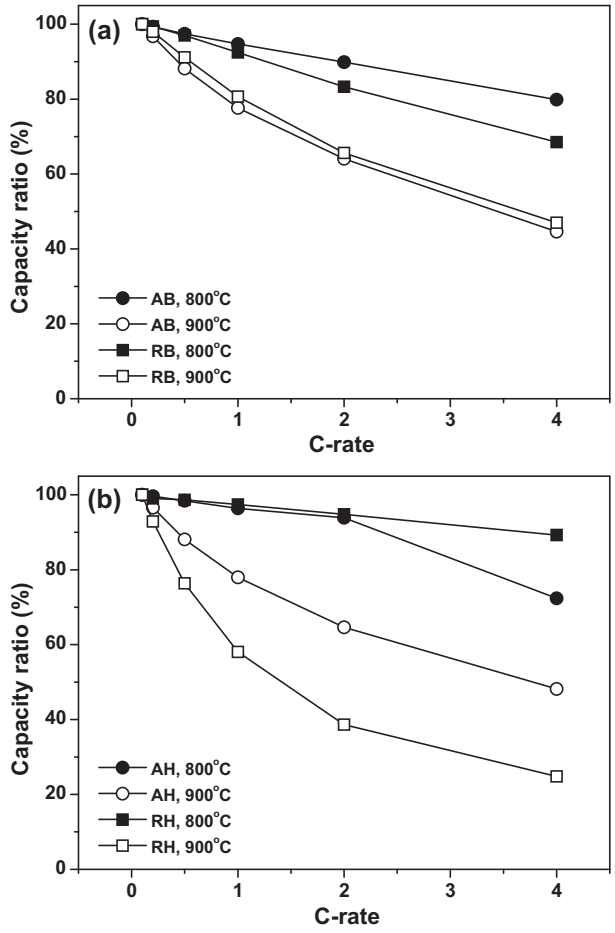


Fig. 11. Normalized capacity as a function of the *C*-rate for $Li_4Ti_5O_{12}$ electrodes prepared by (a) ball milling and (b) high energy milling.

## 4. Conclusions

$Li_4Ti_5O_{12}$ was synthesized by the solid-state reaction between $Li_2CO_3$ and 2 different $TiO_2$ phases for Li-ion battery applications. The following conclusions were made:

1. Heterocoagulated $Li_2CO_3$ and $TiO_2$ particles with high dispersion stability and uniform distribution could be produced during wet milling due to the large difference in zeta potential and different surface charges of the particles.
2. Mechanochemical activation by high energy milling of the starting materials was more effective in decreasing the reaction temperature and particle size as well as increasing the $Li_4Ti_5O_{12}$ content of the final powder than those prepared by conventional ball milling.
3. An anatase- to rutile $TiO_2$ phase transformation was observed at approximately 700 °C, which is lower than the reported values, due to the catalytic effect of $Li_2CO_3$ when anatase $TiO_2$ was used as the starting material. Moreover, this transformed rutile phase was found to react more slowly in a solid-state reaction than the intact rutile $TiO_2$. Therefore, the utilization of rutile $TiO_2$ as a starting phase would be desirable in enhancing the $Li_4Ti_5O_{12}$ content, which is the key factor for increasing the specific capacity.
4. The specific capacities of $Li_4Ti_5O_{12}$ prepared from anatase $TiO_2$ depend significantly on the milling method and heat treatment temperature, whereas those from rutile $TiO_2$ showed a uniform capacity of 160.6–165.1 mAh/g, regardless the change in the main parameters owing to their high $Li_4Ti_5O_{12}$ content.
5. The rate capability of the half cell depended significantly on the $Li_4Ti_5O_{12}$ size, where smaller particles showed higher rate capability due to the short diffusion path and large contact area between the active material and electrolyte.

## Acknowledgements

This study was supported by the Industrial Core Technology Program funded by The Ministry of the Knowledge Economy, Republic of Korea (Project No. 10035302).

## References

[1] K.M. Colbow, J.R. Dahn, R.R. Haering, Structure and electrochemistry of the spinel oxides $LiTi_2O_4$ and $Li_{4/3}Ti_{5/3}O_4$, J. Power Sources 26 (1989) 397–402.
[2] K. Zaghib, M. Armand, M. Gauthier, Electrochemistry of anodes in solid-state Li-ion polymer batteries, J. Electrochem. Soc. 145 (1998) 3135–3140.
[3] A. Guerfi, S. Sévigny, M. Lagacé, P. Hovington, K. Kinoshita, K. Zaghib, Nano-particle $Li_4Ti_5O_{12}$ spinel as electrode for electrochemical generators, J. Power Sources 119–121 (2003) 88–94.
[4] G. Wang, J. Xu, M. Wen, R. Cai, R. Ran, Z. Shao, Influence of high-energy ball milling of precursor on the morphology and electrochemical performance of $Li_4Ti_5O_{12}$ – ball-milling time, Solid State Ionics 179 (2008) 946–950.
[5] A. Guerfi, P. Charest, K. Kinoshita, M. Perrier, K. Zaghib, Nano electronically conductive titanium-spinel as lithium ion storage negative electrode, J. Power Sources 126 (2004) 163–168.
[6] K. Hsiao, S. Liao, J. Chen, Microstructure effect on the electrochemical property of $Li_4Ti_5O_{12}$ as an anode material for lithium-ion batteries, Electrochim. Acta 53 (2008) 7242–7247.
[7] R.F. Nelson, Power requirements for batteries in hybrid electric vehicles, J. Power Sources 91 (2000) 2–26.
[8] B. Scrosati, Challenge of portable power, Nature 373 (1995) 557–558.
[9] G.G. Amatucci, F. Badway, A.D. Pasquier, T. Zheng, An asymmetric hybrid nonaqueous energy storage cell, J. Electrochem. Soc. 148 (2001) A930–A939.
[10] L. Kavan, J. Procházka, T. Spitler, M. Kalváč, M. Zukalová, T. Drezen, M. Grätzel, Li insertion into $Li_4Ti_5O_{12}$ – charge capability vs. particle size in thin-film electrodes, J. Electrochem. Soc. 150 (2003) A1000–A1007.
[11] J.L. Allen, T.R. Jow, J. Wolfenstine, Low temperature performance of nanophase $Li_4Ti_5O_{12}$, J. Power Sources 159 (2006) 1340–1345.
[12] P. Kubiak, A. Garcia, M. Womes, L. Aldon, J. Olivier-Fourcade, P.E. Lippens, J.C. Jumas, Phase transition in the spinel $Li_4Ti_5O_{12}$ induced by lithium insertion influence of the substitutions Ti/V, Ti/Mn. Ti/Fe, J. Power Sources 119–121 (2003) 626–630.
[13] S. Huang, Z. Wen, X. Zhu, Z. Gu, Preparation and electrochemical performance of Ag doped $Li_4Ti_5O_{12}$, Electrochem. Commun. 6 (2004) 1093–1097.
[14] H.E. Park, I.W. Seong, W.Y. Yoon, Electrochemical behaviors of wax-coated Li powder/$Li_4Ti_5O_{12}$ cells, J. Power Sources 189 (2009) 499–502.
[15] G.J. Wang, J. Gao, L.J. Fu, N.H. Zhao, Y.P. Wu, T. Takamura, Preparation and characteristic of carbon-coated $Li_4Ti_5O_{12}$ anode material, J. Power Sources 174 (2007) 1109–1112.
[16] S. Huang, Z. Wen, Z. Zhu, Z. Lin, Effects of dopant on the electrochemical performance of $Li_4Ti_5O_{12}$ as electrode materials for lithium ion batteries, J. Power Sources 165 (2007) 408–412.

[17] H. Kitaura, A. Hayashi, K. Tadanaga, M. Tatsumisago, High-rate performance of all-solid-state lithium secondary batteries using $Li_4Ti_5O_{12}$ electrode, J. Power Sources 189 (2009) 145–148.
[18] B.H. Choi, D.J. Lee, M.J. Ji, Y.J. Kwon, S.T. Park, Study of the electrochemical properties of $Li_4Ti_5O_{12}$ doped with Ba and Sr anodes for lithium-ion secondary batteries, J. Korean Ceram. Soc. 47 (2010) 638–642.
[19] J. Li, Z. Tang, Z. Zhang, Controllable formation and electrochemical properties of one-dimensional nanostructured spinel $Li_4Ti_5O_{12}$, Electrochem. Commun. 7 (2005) 894–899.
[20] S.Y. Yin, L. Song, X.Y. Wang, M.F. Zhang, K.L. Zhang, Y.X. Zhang, Synthesis of spinel $Li_4Ti_5O_{12}$ anode material by a modified rheological phase reaction, Electrochim. Acta 54 (2009) 5629–5633.
[21] T. Yuan, R. Cai, K. Wang, R. Ran, S. Liu, Z. Shao, Combustion synthesis of high-performance $Li_4Ti_5O_{12}$ for secondary Li-ion battery, Ceram. Int. 35 (2009) 1757–1768.
[22] N.A. Alias, M.Z. Kufian, L.P. Teo, S.R. Majid, A.K. Arof, Synthesis and characterization of $Li_4Ti_5O_{12}$, J. Alloys Compd. 486 (2009) 645–648.
[23] S.S. Ryu, D.H. Yoon, Solid-state synthesis of nano-sized $BaTiO_3$ powder with high tetragonality, J. Mater. Sci. 42 (2007) 7093–7099.
[24] D.H. Yoon, Tetragonality of barium titanate powder for a ceramic capacitor application, J. Ceram. Process. Res. 7 (2006) 343–354.
[25] W.S. Jung, H.S. Park, Y.J. Kang, D.H. Yoon, Lowering the sintering temperature of Gd-doped ceria by mechanochemical activation, Ceram. Int. 36 (2010) 371–374.
[26] M.S. Silberberg, Principles of General Chemistry, McGraw Hill, New York, 2007.
[27] H. Matsumoto, D. Nagao, M. Konno, Repetitive heterocoagulation of oppositely charged particles for enhancement of magnetic nanoparticle loading into monodisperse silica particles, Langmuir 26 (2010) 4207–4211.
[28] P.P. Prosini, R.M. Mancini, L. Petrucci, V. Contini, P. Villano, $Li_4Ti_5O_{12}$ as anode in all-solid-state, plastic, lithium-ion batteries for low-power applications, Solid State Ionics 144 (2001) 185–192.
[29] J. Shu, Electrochemical behavior and stability of $Li_4Ti_5O_{12}$ in a broad voltage window, J. Solid State Electrochem. 13 (2009) 1535–1539.
[30] F.C. Gennari, D.M. Pasquevich, Kinetics of the anatase–rutile transformation in $TiO_2$ in the presence of $Fe_2O_3$, J. Mater. Sci. 33 (1998) 1571–1578.
[31] P.S. Ha, H.J. Youn, H.S. Jung, K.S. Hong, Y.H. Park, K.H. Ko, Anatase–rutile transition of precipitated titanium oxide with alcohol rinsing, J. Colloid Interface Sci. 223 (2000) 16–20.
[32] J. Arbiol, J. Cerdà, G. Dezanneau, A. Cirera, F. Peiró, A. Cornet, J.R. Morante, Effects of Nb doping on the $TiO_2$ anatase-to-rutile phase transition, J. Appl. Phys. 92 (2002) 853–861.
[33] S.A. Borkar, S.R. Dharwadkar, Temperatures and kinetics of anatase to rutile transformation in doped $TiO_2$ heated in microwave field, J. Therm. Anal. Calorim. 78 (2004) 761–767.